



Preparation of super activated carbon of vetiver root: optimization by response surface method and study of adsorption behavior on bisphenol A in solution

Guizhen Li^{a,b}, Xiuying Fang^b, Jianmin Li^b, Nianfei Wu^b, Hongbin Wang^b, Xiangyu Wang^{a,*}

^aFaculty of Environmental Science and Engineering, Kunming University of Science and Technology, Kunming 650500, P.R. China, emails: imusthlee2014@sina.com (X. Wang), jiangnanfengyu@126.com (G. Li)

^bSchool of Chemistry and Environment, Yunnan Minzu University, Kunming 650031, P.R. China, emails: ymuhhsyzyx@163.com (X. Fang), wulinfen011@126.com (J. Li), dsddsddj@foxmail.com (N. Wu), wanghb2152@126.com (H. Wang)

Received 29 May 2019; Accepted 31 August 2019

ABSTRACT

Super activated carbon of vetiver root (SAC-VR) was prepared by using potassium hydroxide as an activator. According to the effects of activation time, the mass ratio between KOH and char of vetiver's root (KOH/C ratio) and activation temperature to iodine adsorption, the preparation of SAC-VR was optimized by response surface methodology (RSM). The performances of SAC-VR were investigated by Brunauer–Emmett–Teller (BET), scanning electron microscopy, Fourier transform infrared, thermogravimetric (TG) and X-ray diffraction (XRD). Three parameters of SAC-VR preparation were optimized as follows: activation time was 40 min, activation temperature 936.7°C, and KOH/C ratio 4.98:1. Under the optimized condition, the iodine number of SAC-VR was 1,702 mg/g. The surface of SAC-VR was uneven and had an extensive pore structure. The maximum specific surface area BET was 2,278.27 m²/g, indicating that a large surface area was formed in the activation process of SAC-VR. TG analysis suggests that char of vetiver's root pyrolyzed at 500°C (CHAR) has more cellulose, hemicellulose than SAC-VR. XRD pattern shows that the degree of crystallinity of SAC-VR is lower than that of CHAR. Adsorption behaviors of SAC-VR on bisphenol A (BPA) in the solution were studied. SAC-VR had a good absorption effect on BPA (removal efficiency > 90%). The adsorption process was monolayer adsorption and could be described by the pseudo-second-order kinetic model. SAC-VR could be used in sewage treatment with the solution's pH close to neutral and a novel approach for application of vetiver waste was provided.

Keywords: Super activated carbon; Response surface method; Vetiver root; Activation time; Activation temperature; Bisphenol A

1. Introduction

Vetiveria zizanioides, known as vetiver, is one kind of ideal material controlling ecology and environmental pollution. Its root system has many advantages: rapid growth, thickness, and robustness, toleration of a large range of climatic conditions, etc [1]. Because of its strong adaptive capacity, vetiver can not only grow in different contaminated soil but also remove and absorb high concentration pollutants, particularly. It has obvious removal effects on biochemical

oxygen demand (BOD₅), chemical oxygen demand, total nitrogen and total phosphorus in wastewater in constructed wetlands. Pidatala et al. [2] have studied Pb uptake in vetiver, whose roots accumulate an average of 3,861; 5,132; and 18,562 mg of Pb per kg dry weight in 400, 800, and 1,200 mg/L treated plants, respectively. In the Ogbomoso agricultural zone, Ewetola et al. [3] used vetiver for termite control. Seroja et al. [4] controlled Tofu wastewater using vetiver grass and zeliac. Vetiver root contains vetiver

* Corresponding author.

Presented at the 11th International Conference on Challenges in Environmental Science & Engineering (CESE-2018), 4–8 November 2018, Bangkok, Thailand

alcohol with durable aroma, so vetiver is widely used to produce essential oil for the cosmetics industry. The dispose of scrap material of vetiver generated in production becomes a research hotspot. Gnansounou and Raman [5] produced vetiver biorefineries using straw and vetiver for stopping greenhouse gas emissions. Because vetiver grass has a high degree of cellulose, scrap material of vetiver has been used in both cellulolytic enzyme and bioethanol production [6].

Bisphenol A (BPA) is one of the most representative members of the endocrine-disrupting chemicals family. It has been proved that BPA has weak estrogen-like and strong anti-androgenoid effect, and could interfere with human or animal endocrine system. According to the relevant data, more than 5 million tons of this compound are produced every year [7]. The distribution, migration, transformation and environmental ecological risk of BPA have been the focus of research in recent years.

Scrap material of vetiver has abundant cellulose and lignin, so this paper attempted to prepare super activated carbon of vetiver root (SAC-VR). With pyrolysis temperature 800°C and steam activation, Uras-Postma [8] obtained the methylene blue adsorption of activated carbon (AC) made by vetiver root between 375 and 423 mg/g [8]. There are three activation methods of SAC reported: chemical activation, physical activation [9] and chem-physical activation [10]. The productive process of physical activation has less pollution, but the specific surface area is lower than chemical activation. Chem-physical activation method [11] has a complex process, and could not solve the problem of environmental pollution. The chemical method [12] is one of the most usual and applicable methods for the production of AC. The chemical activator could bring water pollution, but the maturity of the preparation method is better. Various chemical reagents, that is, $ZnCl_2$, H_3PO_4 , and KOH, have been applied in the preparation of AC [13]. $ZnCl_2$ contains the Zn element which is a heavy metal element and using it as activator could lead to secondary pollution [14]. AC made by H_3PO_4 has less specific surface area and could lead to phosphorus pollution. The activation performance of KOH is better than other activators. In the pre-activation process, Molten KOH could keep the surface of AC wet and have good contact with carbon material. In the activation stage, when activation temperature exceeds the boiling point of KOH (762°C), the steam K would pass through carbon material and produce new micropores. Therefore, KOH was used as an activator.

The impact factors of SAC-VR preparation include activation time, activation temperature and the mass ratio between KOH and char of vetiver's root (KOH/C ratio) [15]. In the industrialization process, economic costs, relations of productive rate and performance should be reflected. Searching for the balance of preparation factors is very complex. As one kind of mathematical models with comprehensive experiment design, response surface methodology (RSM) could take a comprehensive research to factors of SAC-VR preparation, and find the interaction of factors and optimal preparation condition. The RSM model could reduce costs, optimize the condition of preparation [16], and is widely used in the field of agriculture, biology, and food.

In this study, the preparation process of SAC-VR was optimized by Controlling activation temperature, activation

time and KOH/C ratio as dependent variables, and the iodine number as response value to fit multiple quadratic regression equations. RSM with Box–Behnken design (BBD) was adopted in preparation. SAC-VR was characterized and analyzed by Brunauer–Emmett–Teller (BET), scanning electron microscopy (SEM), Fourier transform infrared (FT-IR), thermogravimetric (TG) and X-ray diffraction (XRD). The adsorption performance of SAC-VR was evaluated using a hydrophobic pollutant (BPA). The adsorption mechanism of SAC-VR towards BPA was investigated by thermodynamic and kinetic models. This work has demonstrated that SAC-VR has the potential to remove BPA from aqueous solutions under natural conditions.

2. Materials and methods

2.1. Materials

All reagents were of analytical reagent grade. Potassium hydroxide, hydrochloric acid, iodine, and sodium thiosulfate purchased from Wind Reagent Technology Co. Ltd., (Tianjin, China). As shown in Fig. 1, vetiver root was used as raw material obtained from Kunming, Yunnan, China.

2.2. Preparation of AC-VR and SAC-VR

Before the preparation of SAC-VR, the vetiver root was pretreated by washing with deionized water to remove sand. Then, it was dried naturally, cut into pieces and pyrolyzed in muffle oven (YFX-12, purchased from Yifeng electric furnace Co. Ltd., Shanghai, China) to form char of vetiver's root (CHAR) at 500°C for 30 min under nitrogen atmosphere.

Put CHAR into tube furnace holding for 50 min at 850°C with a steam flow rate of 6.5 g/min. Activated carbon made by vetiver root (AC-VR) was produced with the above steps. 6 samples that contained 5 g of CHAR were separately mixed with solutions containing different KOH content. The moisture in the samples was dried for 24 h in a muffle oven at 120°C. The samples were activated at different activation time and activation temperature to determinate the best adsorption result. And then the resultants activated were washed with 0.1 M hydrochloric acid, and the pH value adjusted to 6–7 with distilled water. After being dried in a muffle oven, the final products (SAC-VR) were produced completely [17].



Fig. 1. Raw material of vetiver root for preparation of SAC-VR.

2.3. Iodine adsorption experiment

The iodine number is a technique employed to determine the adsorption capacity of ACs. The iodine number indicates the porosity of the AC and it is defined as the amount of iodine adsorbed by 1 g of carbon at the mg level [18]. Because of the positive correlation between the amount of the micropores of AC and adsorption of iodine on AC [19,20], the iodine number of SAC-VR was measured as follows: SAC-VR was mixed with HCl solution, and then boiled for 30 s. Iodine solution was added when the mixture was cooled down to the room temperature, followed by stirring the solution in thermostatic oscillator (Sanhe instrument Co. Ltd., HGQ45A-11, China) so that iodine could be fully absorbed by the SAC-VR. The mixture was filtered and titrated with an excess sodium thiosulfate solution. The iodine number was calculated based on titration results.

2.4. Optimization of preparation conditions

Batch experiments were used for the optimization of SAC-VR preparation and determining the values of “+1” and “-1” in the Analysis of RSM by the steepest ascent method. Activation temperature was set at 750°C, 800°C, 850°C, 900°C, and 950°C, respectively. KOH/C ratio was from 1:1 to 6:1, and the activation time was from 10 to 50 min. By optimization of preparation, we obtained the direction and steps of the main factors. And then activation temperature, KOH/C ratio and activation time were further optimized by Box–Behnken design of RSM. The Design Expert 8.0.6 software was used to design the BBD model by treating temperature, activation time, KOH/C ratio as X_1 , X_2 , and X_3 , respectively. The regression equation of the optimum condition of preparation was found as follows:

$$Y = \beta_0 + \sum_{i=1}^n \beta_i X_i + \sum_{i=1}^n \beta_{ii} X_i^2 + \sum_{i=1}^{n-1} \sum_{j=i+1}^n \beta_{ij} X_i X_j + \varepsilon \quad (1)$$

where Y is the predicted response iodine number, β_0 is the constant coefficient, β_i is the linear coefficients, β_{ii} is the quadratic coefficients, β_{ij} is the interaction coefficients, ε is error [21,22]. By studying the accuracy of the model by error analysis, the contrast of the significances of factors' influence, ensure that the model can be promoted to the preparation of other waste biomass.

2.5. Characterization of SAC-VR

The information on the surface and pore size of SAC-VR was determined using an automatic volumetric adsorption analyzer (Micromeritics, Model ASAP 2020, USA) to evaluate the adsorption capacity of SAC-VR. The surface morphology and structure were obtained by the SEM analyzer (FEI, Model NOVA NANOSEM 450, USA) without coating. The temperature-dependent weight loss rate was determined by Netzsch STAA49F31 TG. The surface functional groups were tested by the FT-IR spectrometer (NICOLET, Model IS10, Canada) with the transmission method. The number and structure of microcrystalline were measured by an X-ray diffractometer (XRD) analyzer (BROCK, Model D8AA25X, Germany).

2.6. BPA adsorption experiment

The detection method of BPA referenced the research of Ren et al. [23]. Without otherwise specified, adsorption time was 120 min, adsorption temperature was 20°C, adsorbent dose (SAC-VR) was 3 mg, adsorption pH was 7 and 100 mg/L of BPA was 10.00 mL. Studied the effects of pH (from 3 to 11) and adsorbent dose (from 0.2 to 20 mg) on BPA adsorption. Adsorption kinetics was studied at different adsorption time (from 0 to 80 min). Adsorption isotherm curves of 20°C and 30°C were depicted at different concentrations of BPA (20–180 mg/L). Adsorption thermodynamics was also studied by controlling adsorption temperature (from 20°C to 40°C).

3. Results and discussions

3.1. Optimization of preparation conditions

3.1.1. Activation temperature

The mass ratio between KOH and CHAR was 1:1 with 30 min in muffle furnace. The influences of activation temperature ranging from 750°C to 950°C are shown in Table 1. The values of the iodine number increased slowly with the increase of activation temperature. It is because that the CHAR could get sufficient activated at high temperatures. Due to the limitations of the tolerable temperature range of muffle furnace, the influence of temperature above 950°C was not studied. 950°C of temperature was selected as an optimal activation temperature. 750°C and 950°C were chosen as the values of “-1” and “1” of BBD, respectively.

3.1.2. Activation time

When activation temperature was at 950°C and KOH/C ratio 1:1, the heating time for 5 samples was set to be 10, 20, 30, 40, and 50 min, respectively. From Table 2, the adsorption process of SAC-VR increased sharply at the initial stage, and then the adsorption capacity was decreased when heating time over 30 min. With the increase of the activation time, the activator reacted with the microcrystalline structure of carbons, resulting in a decrease in the number of micropores and the adsorption ability of SAC-VR. The optimal activation time was confirmed as 30 min. 10 and 50 min were chosen as the values of “-1” and “1” of BBD, respectively.

3.1.3. KOH/C ratio

KOH was chosen as an activator in this study. The development of the porosity of SAC-VR by KOH is associated with a gasification reaction. KOH is reduced to

Table 1
Iodine number in different activation temperature

| Activation temperature (°C) | Iodine number (mg/g) |
|-----------------------------|----------------------|
| 750 | 657.400 |
| 800 | 750.200 |
| 850 | 826.280 |
| 900 | 932.840 |
| 950 | 942.690 |

Table 2
Iodine number in different activation time

| Activation time (min) | Iodine number (mg/g) |
|-----------------------|----------------------|
| 10 | 675.890 |
| 20 | 885.300 |
| 30 | 928.660 |
| 40 | 915.840 |
| 50 | 925.540 |

metallic potassium by carbon that is oxidized to CO and form a pore structure of SAC-VR during the activation process. The reaction between KOH and carbon occurs according to the following reaction [13]:



The mix ratios of KOH and carbon (CHAR) could affect the specific surface area of SAC-VR. The ratios were as follows: 1:1, 2:1, 3:1, 4:1, 5:1, and 6:1. The mixture was placed into a muffle oven, and then heated under 950°C for 30 min. The results in Table 3 show that the iodine number increased with the increase of the KOH/C ratio. When the ratio was 5:1, the value was 1,750.40 mg/g. Activator (KOH) using in large doses could lead to severe environment pollution [24]. For environment protection and lower usage of KOH, the KOH/C ratio of 5:1 was selected as the optimum ratio. 1:1 and 6:1 were chosen as the values of “-1” and “1” of BBD, respectively.

3.2. Optimization of preparation conditions by RSM

3.2.1. Factor levels design of BBD

From the results of the 3.1 section, activation temperature, activation time and KOH/C ratio were the main factors to the iodine number of SAC-VR. Using the above three factors, the experiments were designed by the BBD method. The results are shown in Table 4.

3.2.2. Analysis of the significance of the regression model

Through the simulation and regression analysis of results of the single-factor (activation temperature, activation time and KOH/C ratio) conditions tested by Design-Expert software, a quadratic regression equation between the iodine number and three factors was obtained as follows:

Table 3
Iodine number in different activation ratio

| KOH/C ratio | Iodine number (mg/g) |
|-------------|----------------------|
| 1:1 | 948.0300 |
| 2:1 | 1096.550 |
| 3:1 | 1584.560 |
| 4:1 | 1672.340 |
| 5:1 | 1750.400 |
| 6:1 | 1630.900 |

Table 4
Experimental programs and results by Box–Behnken design

| No. | A:X ₁ (°C) | B:X ₂ (min) | C:X ₃ (ratio) | Iodine number (mg/g) |
|-----|-----------------------|------------------------|--------------------------|----------------------|
| 1 | 750 | 50 | 3.50 | 1,238.030 |
| 2 | 850 | 30 | 3.50 | 1,360.210 |
| 3 | 850 | 50 | 6.00 | 1,507.600 |
| 4 | 750 | 30 | 6.00 | 926.086 |
| 5 | 750 | 10 | 3.50 | 1,267.970 |
| 6 | 950 | 30 | 6.00 | 1,713.840 |
| 7 | 850 | 10 | 6.00 | 976.454 |
| 8 | 850 | 10 | 1.00 | 771.874 |
| 9 | 850 | 30 | 3.50 | 1,490.560 |
| 10 | 850 | 30 | 3.50 | 1,553.420 |
| 11 | 950 | 30 | 1.00 | 854.188 |
| 12 | 950 | 50 | 3.50 | 1,639.610 |
| 13 | 750 | 30 | 1.00 | 638.358 |
| 14 | 850 | 30 | 3.50 | 1,550.760 |
| 15 | 850 | 30 | 3.50 | 1,461.670 |
| 16 | 950 | 10 | 3.50 | 1,336.110 |
| 17 | 850 | 50 | 1.00 | 947.025 |

$$\text{Iodine number (mg / g)} = -3225.78 + 9.68X_1 - 28.39X_2 - 12.77X_3 + 0.042X_1X_2 + 0.57X_1X_3 + 1.78X_2X_3 - 0.0065X_1^2 - 0.12X_2^2 - 61.59X_3^2 \quad (3)$$

The correlation coefficient of the model R^2 is 0.942; the adjusted correlation coefficient R^2_{adj} is 0.868. Variance results of the regression equation are shown in Tables 5 and 6.

The Model F -value of 12.66 implies the model is significant. There is only a 0.15% chance that a “Model F -value” this large could occur due to noise. Values of “ P -value” less than 0.0500 indicate model terms are significant. The model of the equation is reliable. In this case, A, B, C, AC, and C² are significant model terms. The “Lack of Fit F -value” of 4.10 implies there is a 10.32% chance that a “Lack of Fit F -value” this large could occur due to noise. The P -value of the interaction terms AB and BC are larger than 0.1, indicating that they are not significant, and have no interaction [25].

The analysis results of factor items (X_1 , X_2 , and X_3) and interaction items (X_1X_2 , X_2X_3 , and X_1X_3) are shown in Table 6. The P -values of X_1 , X_2 , X_3 , X_1X_2 , and X_3^2 are smaller than 0.1 and they are regarded as significant items. Fitting equation obtained by significant items is as follows:

$$\text{Iodine number (mg / g)} = 284.03 - 0.16X_1 + 6.12X_2 + 47.66X_3 + 0.57X_1X_3 - 62.60X_3^2 \quad (4)$$

3.3. Analysis of RSM

3.3.1. Analysis of 3D response curve and contour maps

Anyone of activation temperature, activation time and KOH/C ratio was fixed, and the 3D response curve and contour maps could be portrayed by the other factors. The results are as follows:

Table 5
Analysis of variance results of regression equation

| Source | Sum of squares | df | Mean square | F-value | P-value | |
|-------------|--------------------|----|--------------------|---------|---------|-----------------|
| Model | 1.67×10^6 | 9 | 1.85×10^5 | 12.66 | 0.0015 | Significant |
| Residual | 1.02×10^5 | 7 | 14,633.63 | | | |
| Lack of fit | 77,296.00 | 3 | 25,765.33 | 4.10 | 0.1032 | Non-significant |
| Pure error | 25,139.38 | 4 | 6,284.84 | | | |
| Cor. total | 1.77×10^6 | 16 | | | | |

Table 6
Analysis of variance results of factors of regression equation

| Source | Sum of squares | df | Mean square | F-value | P-value |
|----------|----------------|----|-------------|---------|---------|
| X_1 | 271,328.08 | 1 | 271,328.08 | 18.54 | 0.0040 |
| X_2 | 120,014.97 | 1 | 120,014.97 | 8.20 | 0.0240 |
| X_3 | 457,223.77 | 1 | 457,223.77 | 31.24 | 0.0010 |
| X_1X_2 | 27,795.56 | 1 | 27,795.56 | 1.90 | 0.2110 |
| X_1X_3 | 81,774.27 | 1 | 81,774.27 | 5.59 | 0.0500 |
| X_2X_3 | 31,683.11 | 1 | 31,683.11 | 2.17 | 0.1850 |
| X_1^2 | 17,930.49 | 1 | 17,930.49 | 1.23 | 0.3050 |
| X_2^2 | 9,554.83 | 1 | 9,554.83 | 0.65 | 0.4460 |
| X_3^2 | 623,939.52 | 1 | 623,939.52 | 42.64 | 0.0003 |

The direction A and the direction B have a similar inclination in Fig. 2. But the slope is smaller, indicating that the effect of activation time and activation temperature was the same on iodine number.

Fig. 3 shows the influence of activation temperature and KOH/C ratio on the iodine number. While the value of the KOH/C ratio was fixed, the changes in the iodine number were not significant. The iodine number first increased and then decreased with the increase of the KOH/C ratio at the

same temperature. The influence of the KOH/C ratio was more significant than the activation temperature.

From Fig. 4, compared with direction B, the surface curve of C is steeper. The contour density along C is higher than that along B that reveals that KOH/C had a more significant effect on the iodine number. In summary, the KOH/C ratio played the most important role in the adsorption process, the temperature is a secondary factor. Activation time had a minimum impact on adsorption.

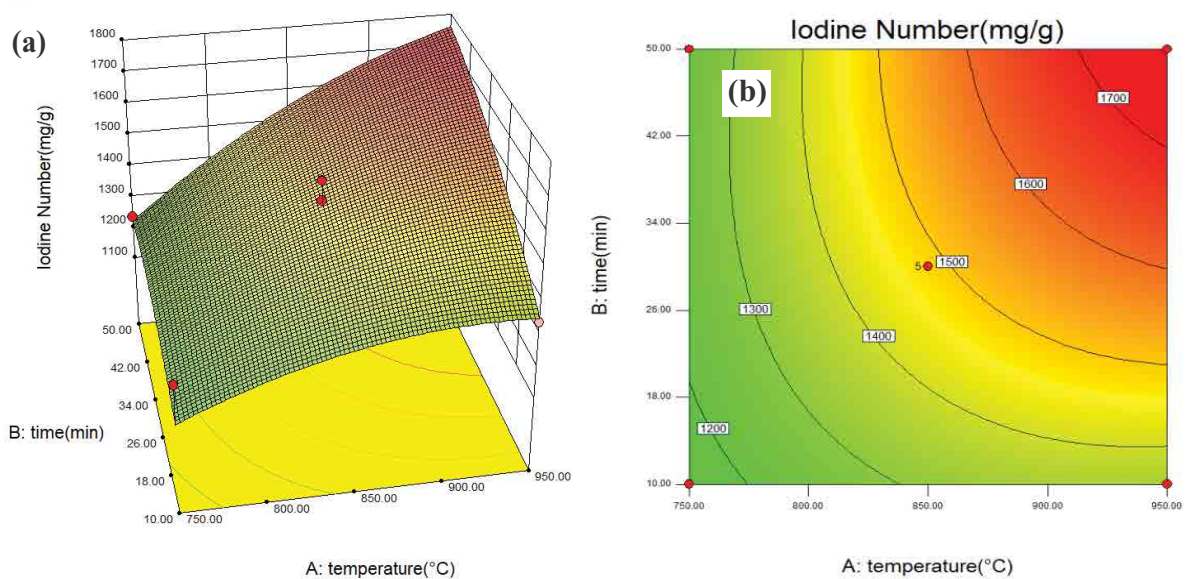


Fig. 2. Influence of activation temperature and activation time on 3D response curve (a) and contour maps (b) of SAC-VR adsorption capacity.

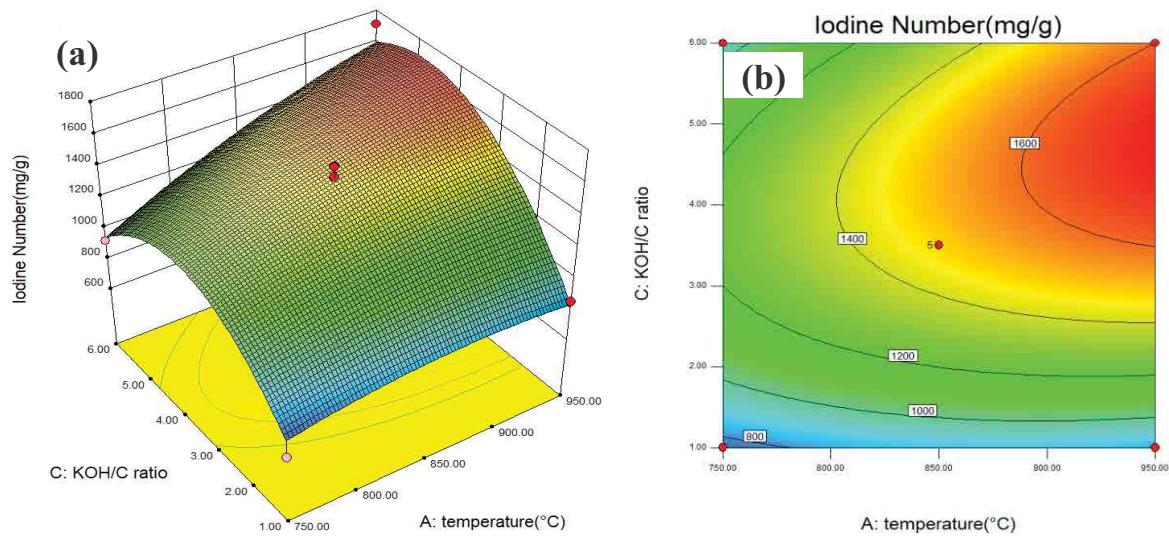


Fig. 3. Influence of activation temperature and KOH/C ratio on 3D response curve (a) and contour maps (b) of SAC-VR adsorption capacity.

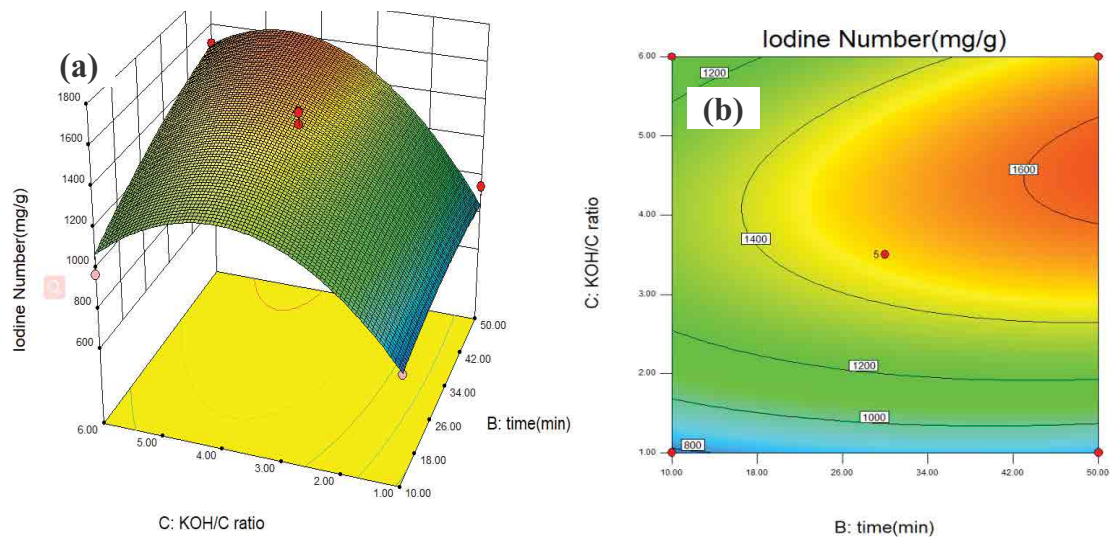


Fig. 4. Influence of activation time and KOH/C ratio on 3D response curve (a) and contour maps (b) of SAC-VR's adsorption capacity.

3.3.2. Factors optimized by RSM and proving experiment

The best values of three key factors, activation temperature, activation time and KOH/C ratio were predicted by the RSM model to be 936.7°C, 40 min, and 4.98:1, respectively. The predicted iodine number was 1,702 mg/g. By the preparation method introduced in Section 2.1 and using the factors optimized by RSM, the experimental value of the iodine number was 1,685 mg/g. Results of the proving experiment coincided with predicted value from the model.

3.4. Characterization of SAC-VR

3.4.1. SEM analysis of apparent appearance

Fig. 5 exhibits the surface structures of SAC-VR before and after activation. Before being activated, the surface of

SAC-VR was smooth and its texture was hard and dense. No porous structures were generated. Fig. 5b shows that the surface of SAC-VR was irregularity and had a well-developed pore structure after activation treatment, which illustrates the activation had significant effects on the formation of porous structures of SAC-VR. This was due to KOH and Carbon reacting to form K_2CO_3 and the reaction promoted the generation of the hole. K_2CO_3 decomposed into K_2O and CO_2 which could drill on the surface of SAC-VR and increased the number of micropores.

3.4.2. BET analysis

The BET analysis results of CHAR and SAC-VR can be seen in Table 7. The results show that 2,278.27 m^2/g of the total specific surface area of SAC-VR reaches the standard

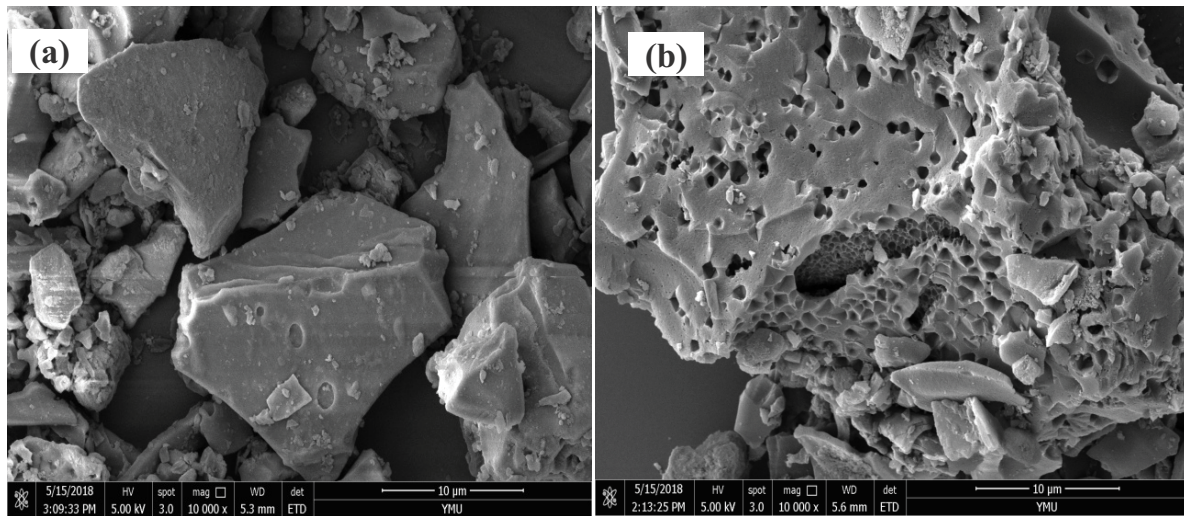


Fig. 5. SEM images of SAC-VR (a) before activation and (b) after activation.

Table 7
BET data of CHAR, AC-VR and SAC-VR

| Parameter | | CHAR | AC-VR | SAC-VR |
|---|-----------------------------------|--------|---------|----------|
| Specific surface area, S_{BET} (m^2/g) | BET | 77.282 | 994.29 | 2,278.27 |
| Micropore specific surface area (m^2/g) | <i>t</i> -plot | – | 835.965 | 1,154.78 |
| External specific surface area (m^2/g) | <i>t</i> -plot | 77.282 | 158.325 | 1,123.49 |
| Total volume (cm^3/g) | Single-point adsorption | 0.3984 | 1.826 | 1.231 |
| Volume of micropore (cm^3/g) | <i>t</i> -plot | – | 0.339 | 0.514 |
| Volume of mesopore (cm^3/g) | Barrett–Joyner–Halenda desorption | 0.08 | 0.086 | 0.205 |
| Average pore size (nm) | – | 5.6053 | 1.9969 | 2.1619 |

of nation ($2,000 \text{ m}^2/\text{g}$). The microporous specific surface area was $1,154.78 \text{ m}^2/\text{g}$, and an external specific surface area was $1,123.49 \text{ m}^2/\text{g}$. Total Volume was $1.231 \text{ cm}^3/\text{g}$, the volume of micropores was $0.514 \text{ cm}^3/\text{g}$ and the average pore size was about 2.1619 nm . The data above reveals that the external specific surface area was larger than the micropore specific surface area and the absorption capacity of SAC-VR came from the external surface. And the value of specific surface area fitted the iodine number measured in this article.

3.4.3. FT-IR analysis

Fig. 6 presents the infrared spectrum of CHAR (a) and SAC-VR (b). It shows that the CHAR spectrum has characteristic peaks of functional groups that do not exist in the SAC-VR spectra. This is due to the breaking of bonds during the activation process, which led to significant changes on the surface of the material.

The peak at $3,400 \text{ cm}^{-1}$ is observed in CHAR and SAC-VR and could be attributed to the O–H stretching vibrations which in the SAC-VR spectra is smaller than that in CHAR. This may be due to the change of water content in the samples. The peaks which appear at $3,250$ and $2,360 \text{ cm}^{-1}$ are characteristic absorption peaks of $\text{C}\equiv\text{C}$. Compared with CHAR, SAC-VR does not have $\text{C}\equiv\text{C}$ functional groups that

indicate that high activation temperature damages the bonds of $\text{C}\equiv\text{C}$ in SAC-VR. The peak near $1,620 \text{ cm}^{-1}$ pertains to stretching vibration absorption of $\text{C}=\text{C}$ bonds in CHAR and SAC-VR. The amount of $\text{C}=\text{C}$ stays the same in the activation process. The peak near $1,440 \text{ cm}^{-1}$ in both CHAR and SAC-VR spectrum can be associated with a $-\text{COO}-$ asymmetric vibration of carboxylic groups [26]. The samples exhibit absorption bands close to $1,040 \text{ cm}^{-1}$, indicating the presence of a C–O single bond, such as that in alcohols, phenols, acids, ethers or esters [26]. The bands around $850\text{--}500 \text{ cm}^{-1}$ can be attributed to C–H and $\text{CH}=\text{CH}_2$ stretching vibrations in aromatic structures. Therefore, after the activation process, the functional groups of SAC-VR were dominated by hydroxyl and carboxylic groups.

3.4.4. TG analysis

As can be seen from Fig. 7, the main weight loss of CHAR and SAC-VR was about 5% and 13% respectively, at $18^\circ\text{C}\text{--}100^\circ\text{C}$. This is caused by water vapor escaping from the material. At this stage, the curve of CHAR declines more quickly than SAC-VR, suggesting there was more water in SAC-VR. After the water had evaporated, the weight loss of SAC-VR was slow and smooth. This is because most organic matter in SAC-VR had been cracked at high temperature

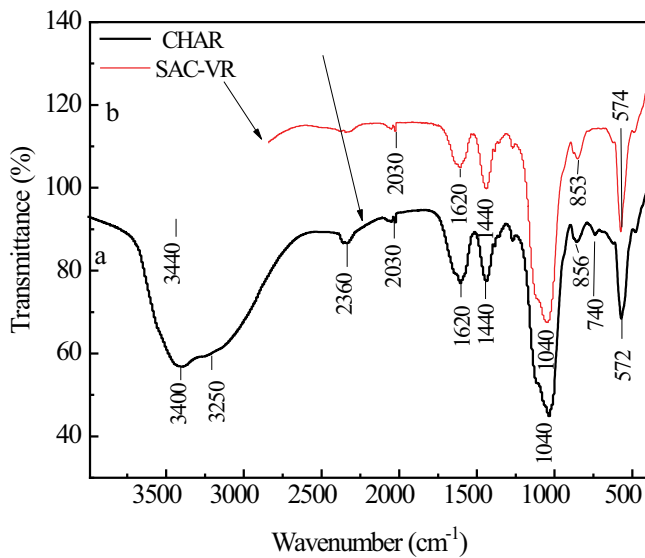


Fig. 6. FT-IR spectra of CHAR (a) and SAC-VR (b).

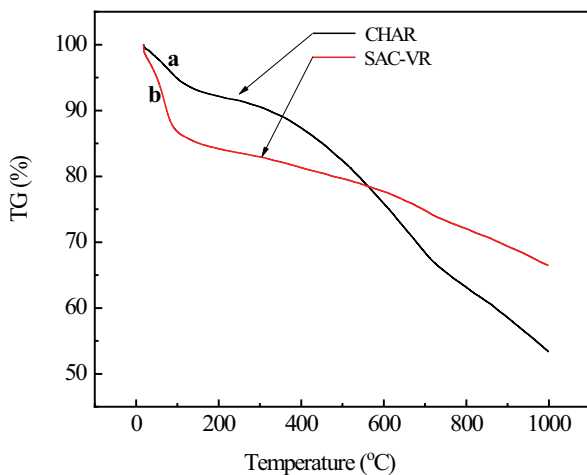


Fig. 7. TG curves of CHAR (a) and SAC-VR (b).

during the activation process. While TG analysis raised to 998°C, SAC-VR lost about 33% of the weight. After TG analysis, the weight loss of CHAR was about 46% and the weight loss of CHAR was quicker and more that indicated the amount of uncracked cellulose, hemicellulose, and lignin in vetiver root CHAR was more than those in SAC-VR. Hemicellulose is pyrolyzed between 250°C and 340°C and the pyrolysis of cellulose is mainly in the range of 300°C–400°C. Therefore, the weight loss speed of CHAR at 700°C slows down, because cellulose and hemicellulose are completely consumed and only a small amount of lignin is cracked. To sum up, CHAR has more cellulose, hemicellulose than SAC-VR.

3.4.5. XRD analysis

The XRD pattern of CHAR has two obvious peaks at $2\theta = 20.79^\circ$ and $2\theta = 26.60^\circ$, respectively (Fig. 8). The peak at 26.60° is the (002) diffraction peak of graphite (PDF

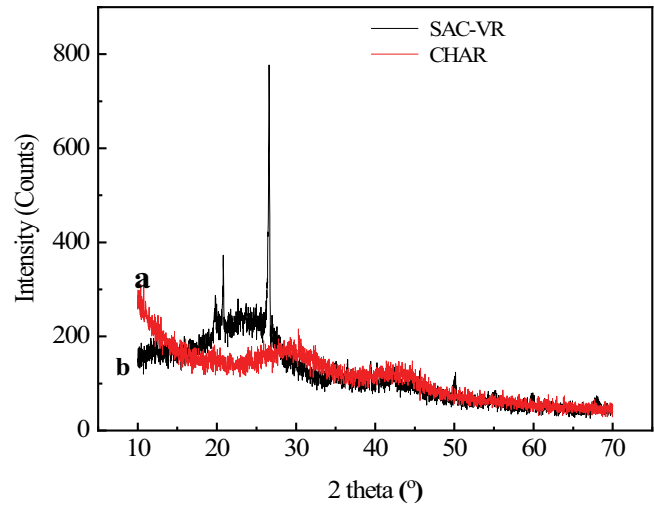


Fig. 8. XRD patterns of CHAR (a) and SAC-VR (b).

#99-0057), indicating that the vetiver root was carbonized, partially graphitized. The peak at 20.79° might be the (100) diffraction peak of silicon dioxide (PDF #79-1906), which maybe come from the surface of the vetiver root. Exclude two peaks above, the XRD pattern of vetiver root is similar to that of SAC-VR. The peak intensity of SAC-VR is weaker, revealing that SAC-VR was with an amorphous structure. The crystal structure of CHAR was destroyed during the activation process by KOH. The degree of crystallinity of SAC-VR was lower than that of CHAR. That is one of the reasons that the adsorption capacity of SAC-VR was higher than that of CHAR.

3.5. Comparison of properties between SAC-VR and ACs prepared by different biomaterials

The adsorptive removal of organic and inorganic substances from wastewater by ACs depends upon the surface area and the pore volume in carbon [27]. From the comparison of properties, different ACs materials listed in Table 8, the surface area of ACs with steam as activator is lower than those activated by chemical method. However, preparation methods using steam as an activator have low pollution. Compared with other chemical activators, SAC-VR has an advantage in specific surface areas. But it has less total pore volume than that of activated carbon using the $ZnCl_2$ activator. Therefore, the adsorption capacity of SAC-VR is higher than those reported in the cited literature.

3.6. BPA adsorption capacity of SAC-VR

3.6.1. Effect of adsorbent dosage

Fig. 9 shows the removal efficiency of BPA with an initial concentration of 100 mg/L by using a different dosage of SAC-VR (0.2, 0.8, 1, 3, 6, 12, and 20 mg) at 20°C. Removal efficiency of BPA increased with increasing SAC-VR dosage at the initial stage. It is because the more dosage of adsorbent provided a bigger surface area and more adsorption sites. There were many vacant sites in the adsorbent at a low dosage of SAC-VR. Concentration gradient between SAC-VR

Table 8
Comparison of AC properties prepared by different biomaterials

| Feedstock | Activator | Surface area, BET (m ² /g) | Total pore volume (cm ³ /g) | Iodine number (mg/g) | References |
|------------------------|--|---------------------------------------|--|----------------------|-------------------|
| Bamboo | Steam | 1,068.00 | 0.550 | – | |
| Camellia nutshell | ZnCl ₂ | 2,023.15 | 2.340 | 1,120.00 | |
| <i>Arundo donax</i> L. | H ₄ P ₂ O ₇ | 1,443.40 | 1.333 | – | |
| Rubber wood sawdust | Steam | 1,092.00 | – | 765.00 | Fang et al. [28] |
| Phenolic resin | Steam | 727.63 | – | 1,050.28 | |
| Camellia nutshell | Steam | 935.00 | – | 968.00 | |
| Acorn shell | Steam-CO ₂ | 1,779 | – | – | Şahin et al. [29] |
| Vetiver root | KOH | 2,278.27 | 1.231 | 1,685 | This work |

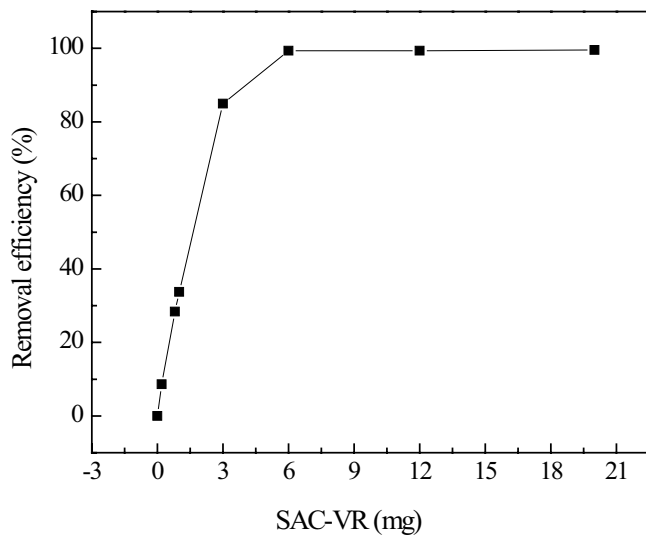


Fig. 9. Influence of adsorbent dosage on BPA adsorption.

and BPA solution were high. As the increase of BPA concentration, adsorption sites were occupied by BPA and removal efficiency decreased slowly. When the dosage of SAC-VR was 6.0 mg, the removal efficiency of BPA could reach 99.35% and the active adsorption sites of SAC-VR were occupied by BPA. Therefore, the adsorption efficiency was maintained at about 99% without obvious change.

3.6.2. Effect of pH

The adsorption capacity exhibits an obvious peak at the solution pH of 7, while adsorption shows a decreasing trend at high pH ranging from 7 to 11 (Fig. 10). It is because that the ionization of BPA occurred at high pH to form the BPA anion and electrostatic repulsion between BPA anion and functional groups on SAC-VR surface led to the reduction of the adsorption capacity of SAC-VR [30].

3.6.3. Adsorption isotherm

Two adsorption models (Langmuir and Freundlich) (Eqs. (5) and (6)) were applied to fit the isothermal adsorption experimental data [28].

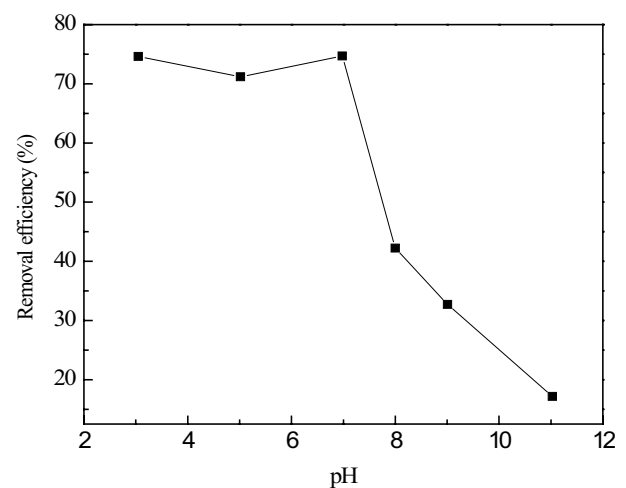


Fig. 10. Influence of solution pH on BPA adsorption.

$$\frac{1}{q_e} = \frac{1}{K_L q_m} \times \frac{1}{C_e} + \frac{1}{q_m} \quad (5)$$

$$\ln q_e = \frac{1}{n} \ln C_e + \ln K_f \quad (6)$$

where C_e (mg/L) is the concentration of BPA at equilibrium, q_e (mg/g) is adsorption of SAC-VR at equilibrium, q_m (mg/g) is the maximum adsorption of SAC-VR at complete coverage, K_L (L/mg) is Langmuir adsorption equilibrium constant, K_f is Freundlich constant and n is Freundlich parameter related to the adsorption intensity.

The fitting curves of the two models are depicted in Fig. 11. And the parameters of the two models are listed in Table 9. From Table 9, the adsorption behavior of SAC-VR could fit to the Langmuir isotherm model due to the highest R^2 , indicating that SAC-VR adsorbing BPA belongs to monolayer adsorption [31]. The maximum adsorption of BPA increased with the rise of temperature.

3.6.4. Thermodynamic studies

By studying the thermodynamic parameters of adsorption, we can have a deeper understanding of the internal

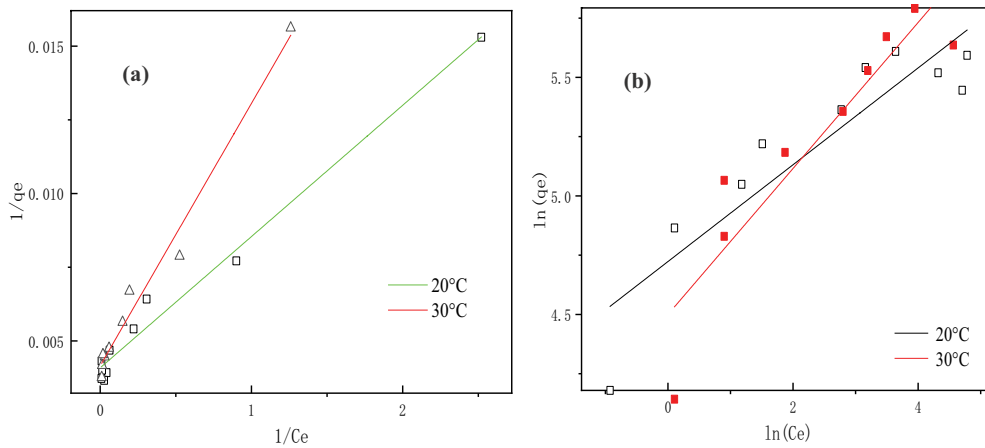


Fig. 11. (a) Langmuir isotherm plots for adsorption of BPA on SAC-VR and (b) Freundlich isotherm plots for the adsorption of BPA on SAC-VR.

Table 9
Langmuir and Freundlich isotherm model parameters

| T (°C) | Langmuir isotherm model | | | | Freundlich isotherm model | | | |
|--------|---------------------------------------|-----------|-----------|----------------|-----------------------------|--------|----------|----------------|
| | Equations | qm (mg/g) | KL (L/mg) | R ² | Equations | 1/n | Kf | R ² |
| 20 | $q_e = \frac{227.27C_e}{1+0.9545C_e}$ | 283.095 | 0.9545 | 0.9831 | $q_e = 112.5053C_e^{1.226}$ | 1.2265 | 112.5053 | 0.8241 |
| 30 | $q_e = \frac{75.33C_e}{1+0.2366C_e}$ | 322.581 | 0.2366 | 0.9466 | $q_e = 89.9901C_e^{1.3607}$ | 1.3607 | 89.9901 | 0.8426 |

energy changes related to the adsorption capacity of SAC-VR on BPA. The thermodynamic parameters include free energy change (ΔG), enthalpy change (ΔH) and entropy change (ΔS). The relationships of parameters are as follows:

$$\Delta G = \Delta H - T\Delta S \tag{7}$$

$$\Delta G = -RT \ln K_c \tag{8}$$

$$\ln K_c = -\frac{\Delta H}{RT} + \frac{\Delta S}{R} \tag{9}$$

where R (8.314 J/mol/K) is ideal gas constant, and T (K) is the reaction temperature. K_c (L/mg) is the adsorption distribution coefficient and it could be calculated by following:

$$K_c = \frac{C_0 - C_e}{C_e} \tag{10}$$

where C_0 (100 mg/L) is the initial concentration of BPA and C_e is the equilibrium concentration of BPA. Function fitting of $\ln K_c$ vs. $-1/T$ is linear, and ΔH and ΔS value are calculated according to the slope and intercept of Eq. (9). ΔG was obtained by Eq. (7).

The effect of different temperatures (293.15, 303.15, and 313.15 K) on the removal of BPA are shown in Table 10.

Table 10
Removal efficiency at different temperature

| Temperature (K) | Ce (mg/L) | Removal efficiency (%) |
|-----------------|-----------|------------------------|
| 293.15 | 25 | 75 |
| 303.15 | 28.57 | 71.43 |
| 313.15 | 31.35 | 68.65 |

Table 11
Thermodynamic parameters for adsorption of BPA on SAC-VR

| Temperature (K) | ΔG (J/mol) | ΔH (J/mol) | ΔS (J/mol/K) |
|-----------------|--------------------|--------------------|----------------------|
| 293.15 | -2,766.46 | -17,004.62 | -48.57 |
| 303.15 | -2,280.76 | -17,004.62 | -48.57 |
| 313.15 | -1,795.07 | -17,004.62 | -48.57 |

The thermodynamic parameters calculated are listed in Table 11.

$\Delta G < 0$, indicates that adsorption was spontaneous. With the system temperature increasing, ΔG was declined, which suggests the decreasing trend of adsorption [32]; $\Delta H < 0$ indicates that the adsorption reaction was exothermic, which was consistent with the results where the BPA uptake increased with the increasing solution temperature [33]. ΔH less than 20.9 kJ/mol suggests that the adsorption process of BPA

Table 12
Pseudo-first and pseudo-second-order kinetic model parameters

| T (°C) | Pseudo-second-order | | | | Pseudo-first-order | | | |
|--------|---------------------|-------------|-------------|-----------------------|--------------------|-------------|-------------|-----------------------|
| | q_e (mg/g) | k_1 (min) | R^2_{adj} | P | q_e (mg/g) | k_2 (min) | R^2_{adj} | P |
| 20 | 244.8036 | 0.0353 | 0.8750 | 1.9×10^{-15} | 228.9784 | 208.9405 | -0.0909 | 2.8×10^{-10} |

was physical adsorption [32]. The exothermic processes of adsorption could be caused by increasing the rate of diffusion of the adsorbate molecules across the external boundary layer; the degree of randomness decreased due to $\Delta S < 0$.

3.6.5. Adsorption kinetics studies

Pseudo-first and pseudo-second-order kinetic models [34] were used for kinetic analysis about the relationship between SAC-VR dosage and adsorption capacity of BPA. The equations of two models were fitted by non-linear equations [31].

$$\ln(q_e - q_t) = \ln(q_e) - k_1 t \quad (11)$$

$$\frac{t}{q_t} = \frac{1}{k_2 q_e^2} + \frac{t}{q_e} \quad (12)$$

where q_e (mg/g) is the amount of BPA adsorbed at equilibrium, q_t (mg/g) is the amount of BPA adsorbed at time t (min), and k_1 (min) and k_2 (g/mg/min) are equilibrium rate constant of pseudo-first and pseudo-second-order adsorption, respectively. The results are listed in Table 12. By comparison of the correlation coefficients R^2_{adj} of two kinetic models, the pseudo-second-order kinetic model has better data correlation, indicating that the adsorption process of BPA confirmed to the second-order kinetic model. The maximum adsorption capacity was 244.8036 mg/g at 20°C.

4. Conclusions

SAC-VR was prepared by using vetiver root. The preparation process of SAC-VR was optimized by BBD. The results of single-factor experiments and RSM model show that the predicted value of three important factors for RSM model activation temperature, activation time and KOH/C ratio was 937.5°C, 49.1 min and 5.24:1, respectively. The relevant iodine number was 1,702 mg/g. The total specific surface area was 2,360.01 m²/g measured by BET. Experimental results coincide with the results predicted by the model. The SEM and BET analysis results indicated that SAC-VR optimized by RSM with well-developed porous structure and high specific surface area. And the model could be popularized for the study of preparation of other SAC. The removal efficiency of BPA could be as high as 99.35%. By studying the adsorption behavior of thermodynamics and dynamics, the adsorption process was monolayer adsorption and could be described by Pseudo-second-order kinetic model. This paper provides a promising method for the application of vetiver waste.

Acknowledgments

This work was supported by the National Key Research and Development Program of China (Grant No. 2018YFC1900301) and the National Natural Science Foundation of China (Grant No. 51968031).

References

- [1] J.K. Raman, C.M. Alves, E. Gnansounou, A review on moringa tree and vetiver grass – potential biorefinery feedstocks, *Bioresour. Technol.*, 249 (2017) 1044–1051.
- [2] V.R. Pidatala, K. Li, D. Sarkar, R. Wusirika, R. Datta, Comparative metabolic profiling of vetiver (*Chrysopogon zizanioides*) and maize (*Zea mays*) under lead stress, *Chemosphere*, 193 (2018) 903–911.
- [3] E.A. Ewetola, S.A. Babarinde, T. Omirin and D.O. Ojewole, Farmers' perception of the usefulness of vetiver grass for termite control on Ogbomoso agricultural zone farmlands, south-western Nigeria, *J. King Saud Univ. – Sci.*, 30 (2017) 214–222.
- [4] R. Seroja, H. Effendi, S. Hariyadi, Tofu wastewater treatment using vetiver grass (*Vetiveria zizanioides*) and zeliac, *Appl. Water Sci.*, 8 (2018) 1–6.
- [5] E. Gnansounou, J.K. Raman, Environmental performances of coproducts. application of claiming-based allocation models to straw and vetiver biorefineries in an Indian context, *Bioresour. Technol.*, 262 (2018) 203–211.
- [6] K. Subsamran, P. Mahakhan, K. Vichitphan, S. Vichitphan, J. Sawaengkaew, Potential use of vetiver grass for cellulolytic enzyme production and bioethanol production, *Biocatal. Agric. Biotechnol.*, 17 (2019) 261–268.
- [7] H. Zhu, Z. Li, J. Yang, A novel composite hydrogel for adsorption and photocatalytic degradation of bisphenol A by visible light irradiation, *Chem. Eng. J.*, 334 (2018) 1679–1690.
- [8] Ü. Uras-Postma, M. Carrier, J. (Hansie) Knoetze, Vacuum pyrolysis of agricultural wastes and adsorptive criteria description of biochars governed by the presence of oxides, *J. Anal. Appl. Pyrolysis*, 107 (2014) 123–132.
- [9] K.F. Fu, Q.Y. Yue, B.Y. Gao, Y. Wang, Q. Li, Activated carbon from tomato stem by chemical activation with FeCl₃, *Colloids Surf., A*, 529 (2017) 842–849.
- [10] G.Z. Li, J.X. Li, W. Tan, H. Jin, H.X. Yang, J.H. Peng, C.J. Barrow, M. Yang, H.B. Wang, W.R. Yang, Preparation and characterization of the hydrogen storage activated carbon from coffee shell by microwave irradiation and KOH activation, *Int. Biodeterior. Biodegrad.*, 113 (2016) 386–390.
- [11] H. Laksaci, A. Khelifi, B. Belhamdi, M. Trari, Valorization of coffee grounds into activated carbon using physic–chemical activation by KOH/CO₂, *J. Environ. Chem. Eng.*, 5.5 (2017) 5061–5066.
- [12] A. Bazan-Wozniak, P. Nowicki, R. Pietrzak, Production of new activated bio-carbons by chemical activation of residue left after supercritical extraction of hops, *Environ. Res.*, 161 (2018) 456–463.
- [13] T. Tay, S. Ucar, S. Karagöz, Preparation and characterization of activated carbon from waste biomass, *J. Hazard. Mater.*, 165 (2009) 481–485.
- [14] H. Dolas, O. Sahin, C. Saka, H. Demir, A new method on producing high surface area activated carbon: the effect of salt on the surface area and the pore size distribution of activated carbon prepared from pistachio shell, *Chem. Eng. J.*, 166 (2011) 191–197.

- [15] X. Fang, G. Li, J. Li, H. Jin, J. Li, V. Jegatheesan, M. Yang, Bamboo charcoal derived high-performance activated carbon via microwave irradiation and KOH activation: application as hydrogen storage and super-capacitor, *Desal. Wat. Treat.*, 96 (2017) 120–127.
- [16] M. Danish, T. Ahmad, W.N.A.W. Nadhari, M. Ahmad, W.A. Khanday, Z. Lou, Z. Pin, Optimization of banana trunk-activated carbon production for methylene blue-contaminated water treatment, *Appl. Water Sci.*, 8 (2018) 1–11.
- [17] S.J. Li, K.H. Han, J.X. Li, M. Li, C.M. Lu, Preparation and characterization of super activated carbon produced from gulfweed by KOH activation, *Microporous Mesoporous Mater.*, 243 (2017) 291–300.
- [18] C. Saka, BET, TG–DTG, FT-IR, SEM, iodine number analysis and preparation of activated carbon from acorn shell by chemical activation with ZnCl₂, *J. Anal. Appl. Pyrolysis*, 95 (2012) 21–24.
- [19] W.Y. Ao, J. Fu, X. Mao, Q.H. Kang, C.M. Ran, Y. Liu, H.D. Zhang, Z.P. Gao, J. Li, G.Q. Liu, J.J. Dai, Microwave assisted preparation of activated carbon from biomass: a review, *Renewable Sustainable Energy Rev.*, 92 (2018) 958–979.
- [20] W. Jiang, X.J. Xing, S. Li, X.W. Zhang, W.Q. Wang, Synthesis, characterization and machine learning based performance prediction of straw activated carbon, *J. Cleaner Prod.*, 212 (2018) 1210–1223.
- [21] Q.F. Yu, H.R. Zhao, H. Zhao, S.N. Sun, X. Ji, M. Li, Y.F. Wang, Preparation of tobacco-stem activated carbon from using response surface methodology and its application for water vapor adsorption in solar drying system, *Sol. Energy*, 177 (2019) 324–336.
- [22] Y.J. Meng, X.Z. Wang, Z.G. Wu, S.Q. Wang, T.M. Young, Optimization of cellulose nanofibrils carbon aerogel fabrication using response surface methodology, *Eur. Polym. J.*, 73 (2015) 137–148.
- [23] J.Q. Ren, D.B. Jia, Y.F. Zhuang, Determination of bisphenol-A in plastic product using ultraviolet adsorption spectroscopy, *J. Jilin Inst. Chem. Technol.*, 24 (2007) 40–42.
- [24] V. Montes, J.M. Hill, Activated carbon production: recycling KOH to minimize waste, *Mater. Lett.*, 220 (2018) 238–240.
- [25] N.S. Sulaiman, R. Hashim, M.H.M. Amini, M. Danish, O. Sulaiman, Optimization of activated carbon preparation from cassava stem using response surface methodology on surface area and yield, *J. Cleaner Prod.*, 198 (2018) 1422–1430.
- [26] K.C. Bedin, A.C. Martins, A.L. Cazetta, O. Pezoti, V.C. Almeida, KOH-activated carbon prepared from sucrose spherical carbon: adsorption equilibrium, kinetic and thermodynamic studies for methylene blue removal, *Chem. Eng. J.*, 286 (2016) 476–484.
- [27] C. Saka, Ö. Şahin, M.M. Küçük, Applications on agricultural and forest waste adsorbents for the removal of lead (II) from contaminated waters, *Int. J. Environ. Sci. Technol.*, 9 (2012) 379–394.
- [28] X.Y. Fang, M. Yang, J.X. Li, M. Xiang, K. Yang, H.B. Wang, G.Z. Li, Preparation of bamboo activated carbon by microwave radiation with water vapour activation and investigation of its adsorption properties, *Desal. Wat. Treat.*, 135 (2018) 351–361.
- [29] Ö. Şahin, C. Saka, Preparation and characterization of activated carbon from acorn shell by physical activation with H₂O–CO₂ in two-step pretreatment, *Bioresour. Technol.*, 136 (2013) 163–168.
- [30] W.-T. Tsai, H.-C. Hsu, T.-Y. Su, K.-Y. Lin, C.-M. Lin, Adsorption characteristics of bisphenol-A in aqueous solutions onto hydrophobic zeolite, *J. Colloid Interface Sci.*, 299 (2006) 513–519.
- [31] L.H. Velazquez-Jimenez, J.A. Arcibar-Orozco, J.R. Rangel-Mendez, Overview of As(v) adsorption on Zr-functionalized activated carbon for aqueous streams remediation, *J. Environ. Manage.*, 212 (2018) 121–130.
- [32] X. Hu, H. Zhang, Z.R. Sun, Adsorption of low concentration ceftazidime from aqueous solutions using impregnated activated carbon promoted by iron, copper and aluminum, *Appl. Surf. Sci.*, 392 (2017) 332–341.
- [33] I.W.A. Tan, A.L. Ahmad, B.H. Hameed, Adsorption isotherms, kinetics, thermodynamics and desorption studies of 2,4,6-trichlorophenol on oil palm empty fruit bunch-based activated carbon, *J. Hazard. Mater.*, 164 (2009) 473–482.
- [34] M. Özdemir, Ö. Durmuş, Ö. Şahin, C. Saka, Removal of methylene blue, methyl violet, rhodamine B, alizarin red, and bromocresol green dyes from aqueous solutions on activated cotton stalks, *Desal. Wat. Treat.*, 57 (2016) 18038–18048.